Available online at www.sciencedirect.com

ScienceDirect

Procedia Engineering 105 (2015) 381 – 387

Procedia Engineering

www.elsevier.com/locate/procedia

6th BSME International Conference on Thermal Engineering (ICTE 2014)

Analysis of Heat Transfer and Entropy Generation of TiO_2-Water Nanofluid Flow in a Pipe under Transition

Goutam Saha and Manosh C. Paul*

Systems, Power and Energy Research Division, School of Engineering,
University of Glasgow, Glasgow G12 8QQ, UK

Abstract

Single and multi-phase numerical simulations are carried out to investigate the heat transfer and entropy generation behaviour of transitional flow of TiO_2−H_2O nanofluid in a circular pipe. Results reveal that the small diameter of nanoparticles has the highest heat transfer rate for χ = 6% and the TiO_2-water nanofluid shows higher heat transfer rate using multi-phase model compared to that of the single phase model. Also no optimal Reynolds has been observed which could minimise the total entropy generation. New correlations are proposed to calculate the average Nusselt number using a nonlinear regression analysis with a standard deviation of error of less than 0.5%.

Peer-review under responsibility of organizing committee of the 6th BSME International Conference on Thermal Engineering (ICTE 2014)

Keywords: Nanofluid; heat transfer; entropy generation; single phase model; multi-phase model;

1. Introduction

Industries developing technology related to heat transfer are more concern on the design of new thermal systems, thus research is in progress to investigate the hydrodynamic and heat transfer behaviour of new forms of heat transfer fluid such as one called nanofluid. Choi [1] first used nanofluid and verified that the addition of nanoparticles into a base fluid helps to increase the thermal conductivity and hence enhances the heat transfer rate of nanofluid. Several experimental and numerical investigations have also been carried out by researchers to investigate the effect of nanoparticle size diameters, volume concentrations and different nanofluids on the heat transfer behaviour in a circular pipe in laminar flow regime using single and multi-phase models, as reported in [2-15]. However, a very few experimental works of nanofluid have been found in transition flow regime [16, 17].

*Corresponding author. Tel.: +44(0)141 330 8466; fax: +44(0)141 330 4343.
Email address: Manosh.Paul@glasgow.ac.uk (M.C. Paul)

Peer-review under responsibility of organizing committee of the 6th BSME International Conference on Thermal Engineering (ICTE 2014)
doi:10.1016/j.proeng.2015.05.023

To the best of our knowledge, no research has been carried out to-date to understand the transitional behaviour of heat transfer and total entropy generation of the TiO_2–water nanofluid in a circular pipe. Hence, the objective of our study is to analyse this using both single and multi-phase models.

2. Governing Equations

Two-dimensional axi-symmetric model of a horizontal circular pipe with a length (L) of $1.0\ m$ and a circular section with diameter, D_h, of $0.019\ m$ is considered as shown in Fig. 1. The dimensional steady state governing equations for the fluid flow and heat transfer for the single- and multi-phase models can be expressed as (Fluent [18]):

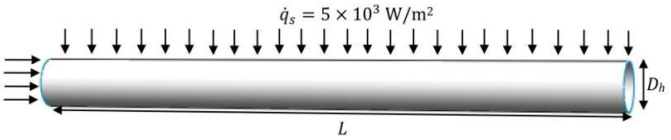

Figure 1: Schematic diagram of the geometry under consideration

Single Phase Model (SPM)

$$\nabla.\left(\rho_m \vec{V}_m\right) = 0 \tag{1}$$

$$\nabla.\left(\rho_m \vec{V}_m \vec{V}_m\right) = -\nabla P_m + \nabla.\left[\mu_m \nabla \vec{V}_m - \sum_{s=1}^{n} \chi_s \rho_s \overline{v_s}\ \overline{v_s}\right] \tag{2}$$

$$\nabla.\left(\rho_m \vec{V}_m C_p T\right) = \nabla.\left(\lambda_m \nabla T - C_p\ \rho_m \overline{vt}\right) \tag{3}$$

Multi-phase Mixture Model (MPM)

$$\nabla.\left(\rho_m \vec{V}_m\right) = 0 \tag{4}$$

$$\nabla.\left(\rho_m \vec{V}_m \vec{V}_m\right) = -\nabla P_m + \nabla.\left[\mu_m \nabla \vec{V}_m - \sum_{s=1}^{n} \chi_s \rho_s \overline{v_s}\ \overline{v_s}\right] + \nabla.\left(\sum_{s=1}^{n} \chi_s \rho_s \vec{V}_{dr,s}\ \vec{V}_{dr,s}\right) \tag{5}$$

$$\nabla.\left[\sum_{s=1}^{n} \chi_s \vec{V}_s (\rho_s H_s + P_m)\right] = \nabla.\left(\lambda_m \nabla T - C_p \rho_m \overline{vt}\right) \tag{6}$$

$$\nabla.\left(\chi_p\ \rho_p \vec{V}_m\right) = -\nabla.\left(\chi_p\ \rho_p \vec{V}_{dr,p}\right) \tag{7}$$

The equations for the kinetic energy (κ) and specific dissipation rate of kinetic energy (ω) used in the SST $\kappa - \omega$ model are given by [19]

$$div\left(\rho_m \kappa \vec{V}_m\right) = div\left\{\left(\mu_m + \frac{\mu_{t,m}}{\sigma_k}\right) grad\ \kappa\right\} + G_\kappa - \rho_m \kappa\omega\ \beta_1 \tag{8}$$

$$\begin{aligned} div\left(\rho_m \omega \vec{V}_m\right) &= div\left\{\left(\mu_m + \frac{\mu_{t,m}}{\sigma_\omega}\right) grad\ \omega\right\} + G_\omega - \rho_m \omega^2 \beta_2 \\ &+ 2(1 - F_1)\rho_m\ \sigma_{\omega,2}\ \frac{grad\ \omega\ grad\ \kappa}{\omega} \end{aligned} \tag{9}$$

The total entropy generation equation for a circular pipe of length L is proposed by Ratts and Raut [20] and defined as

$$E_{gen} = \frac{\pi D_h^2\ L\ \dot{q}_s^2}{\lambda_{nf}\ \overline{Nu}\ T_{avg}} + \frac{32 \dot{m}^3 f L}{\rho_{nf}^2 \pi^2 D_h^5\ T_{avg}} \tag{10}$$

At the pipe inlet, a uniform velocity and a uniform temperature $T_{in} = 293\ K$, with a constant intensity $I = 3\%$ based on the hydraulic diameter, $D_h = 0.019\ m$ have been stated. At the pipe outlet, a pressure outlet boundary condition has been specified. On the pipe wall, a no-slip boundary condition is introduced and uniform heat flux

boundary condition has been implemented. Also, further details about the thermophysical properties of nanofluid, base fluid (water) and nanoparticles could be found in our recent publication, Saha and Paul [21].

3. Results and Discussion

Numerical simulations are carried out with $Re = 2300$ to 10×10^3, $Pr = 7.04$ to 20.29, $\chi = 0$ to 6%, and $d_p = 10$ to $40\ nm$. The governing non-linear partial differential equations for the continuity, momentum, energy and other scalars together with the suitable boundary conditions are discretised and hence solved by using the Finite volume solver Fluent 6.3. For all the simulations carried out in the present analysis, convergence criteria for the solutions are considered when the residuals become less than 10^{-8}.

The grid sensitivity test is carried out by varying the total number of grid distributions in both the axial *(Nx)* and radial *(Nr)* directions. It is found that the grid $Nx = 500 \times Nr = 100$ generate most reasonable result. In order to validate the accurateness of the present numerical findings, validation has been done for the base fluid (water) against the existing experimental data values as well as correlations for different $Re = 2300$ to 10^4 and $Pr = 7.04$. Figure $2(a)$ shows the variation of the Darcy friction factor between the present result and the correlation of Blasius [22] and other experimental results of Chandrasekar *et al.* [14] and Naik *et al.* [15]. Maximum deviation of 10.35% for $Re = 2300$ and minimum deviation of 0.17% are observed for $Re = 10 \times 10^3$. Also from Fig. 2(b), it is observed that the maximum deviation between the present average Nusselt number result and the Gnielinski equation [23] is 28.75% for $Re = 3100$. Also, the maximum deviation between our average Nusselt number result and the experimental result of Naik *et al.* [15] is 2.01% for $Re = 2291$ which shows very good agreement with the experimental result. The reason behind such small variation may be due to the near wall mesh distribution and temperature gradient at the wall. At the end, it is to be assumed that the present predictions are realistic for $Re = 2300$ to 10^4 under transition flow regime.

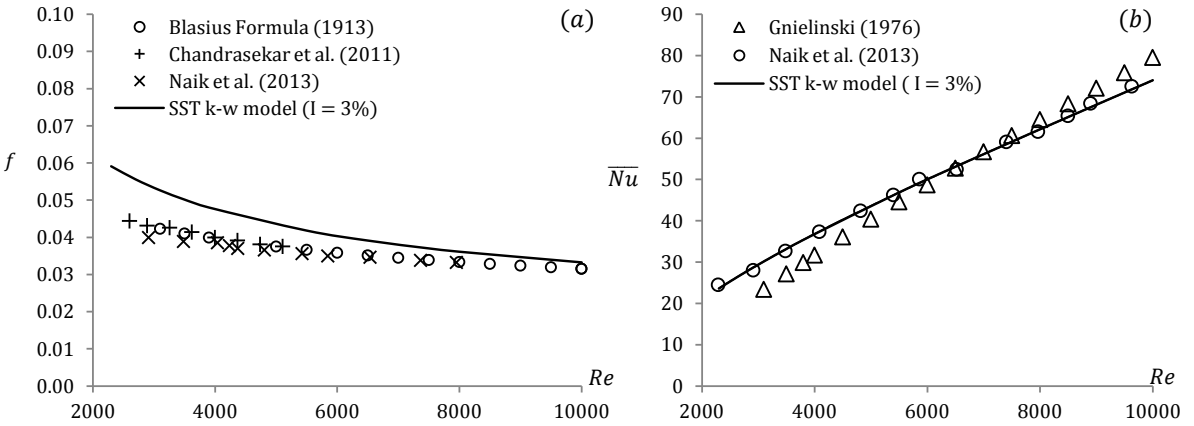

Figure 2: Comparison of the (a) Darcy friction factor, *f* and (b) average Nusselt number, $\overline{Nu}$ of the base fluid (water) with different correlations and experimental results for different Re

3.1 Local and average heat transfer analysis

Figure 3a shows the axial variation of local Nusselt number for TiO_2-water nanofluid with $d_p = 10\ nm$ and $\chi = 2\%$. From this figure, it is easy to locate the critical distance measured from the upstream where the transition actually begins. It is also observed that the enhancement of local Nusselt number increases in the entrance region and then rapidly decreases with the axial distance until a minimum value can be predicted from the breakdown of laminar flow. When this minimum value is achieved, Nusselt number started to rise again and then reaches a constant value as the flow tends to be fully developed. It is also found that critical distance is strongly dependent on the Reynolds number. As the Reynolds number increases, such critical distance decreases monotonically. Moreover,

the critical distance moves to a distance close to the upstream of the pipe when the Reynolds number increases from 2300 to 10×10^3 and then it tends to vanish for the Reynolds number greater than 10×10^3. It means that there is a laminar state between the upstream and the breakdown point. This outcomes also strongly support the observations made by Abraham *et al.* [24].

Figures 3b shows the variation of average Nusselt number with the Reynolds number for different nanoparticles volume concentrations of TiO_2-water nanofluids using both single phase model (SPM) and multi-phase model (MPM). The results indicate that the average Nusselt number monotonically increases with the increase of nanoparticle volume concentration. It is also observed that higher average Nusselt number is achieved using the multi-phase model than the single-phase model. This is due to the slip velocity which may not be zero when the interaction between the fluid and particle phase is considered. This variation becomes more significant for higher nanoparticle volume concentrations as well as small nanoparticle size diameters. This is noteworthy because of rapid movement of smaller nanoparticles within the fluid. Particularly for the single phase model, TiO_2–water nanofluid and $\chi = 2\%$, 4% and 6% with $d_p = 10\,nm$, the maximum percentage enhancement is approximately 3.29, 11.34 and 29.34 respectively, while for multi-phase model, it is approximately 3.50, 12.37 and 31.24 respectively.

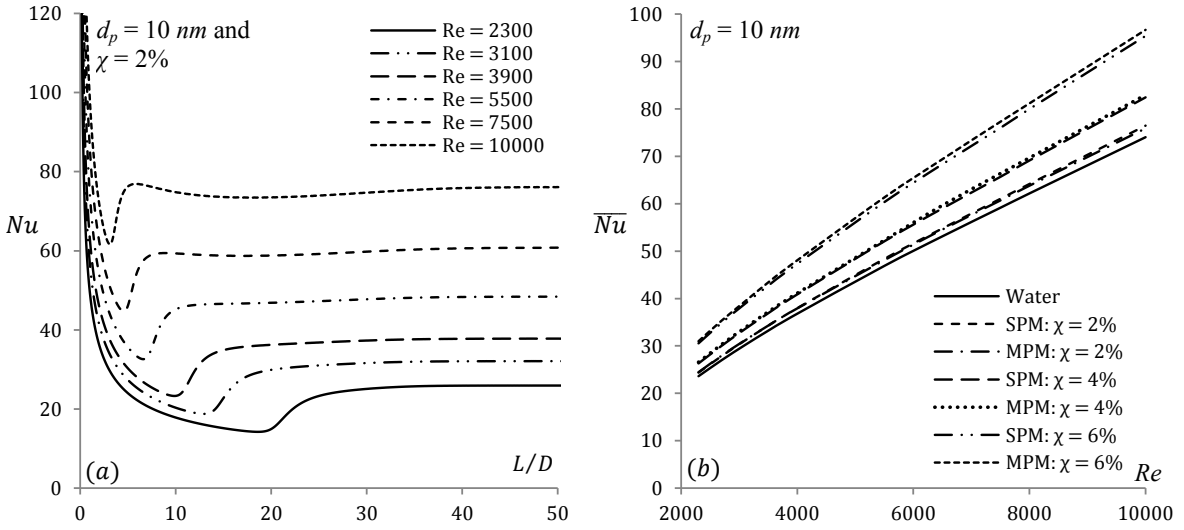

Figure 3: Variation of local and average Nusselt number of TiO_2-H_2O nanofluid for different *Re*

3.2 Entropy generation analysis

Figure 4 show the variation of the total entropy generation for TiO_2-water nanofluids using both single phase and multi-phase model. It is seen that the total entropy generation decreases as the Reynolds number increases with the decrease of the nanoparticles size diameter. Also, insignificant effect of frictional entropy generation on total entropy generation is observed for different nanoparticles size diameter and volume concentration. Particularly for $\chi = 2\%$ and TiO_2-water nanofluid, total entropy generation rapidly decreases as the Reynolds number increases. This occurs due to the enhancement of average Nusselt number and increase of thermal conductivity of nanofluid. Also, the rapid reduction of total entropy generation means that effect of friction entropy generation is negligible and the effect of thermal entropy generation becomes more significant. It shows, the behaviour of thermal entropy generation is similar to total entropy generation. On the other hand, it is observed that increases in nanoparticles volume concentration make an impact on total entropy generation being reduced. Moreover, total entropy generation decreases as the nanoparticles size diameter decrease. This happens due to the significant increase of heat transfer rate as well as the increase of thermal conductivity of nanofluids too. However, no optimal Reynolds has been observed which could minimize the total entropy generation.

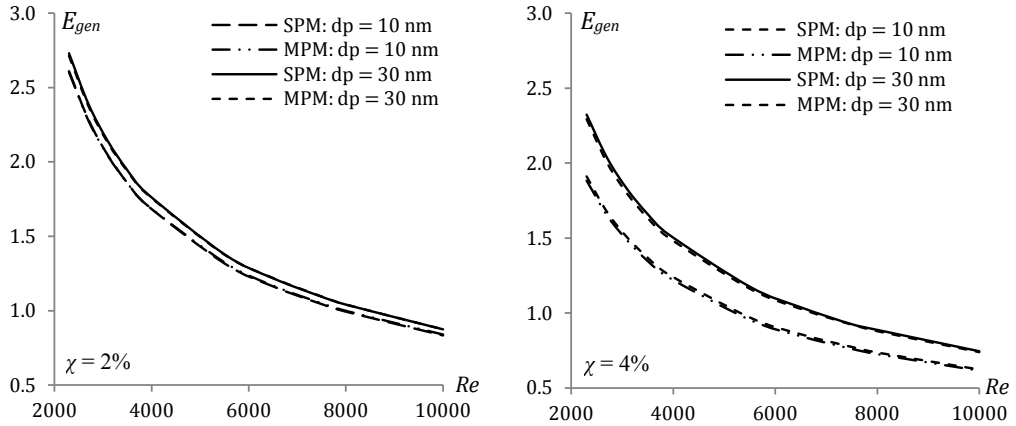

Figure 4: Variation of total entropy generation with different Reynolds number for TiO_2-water nanofluid

3.3 Correlations

By using the non-linear regression analysis, following correlations have been proposed with maximum standard deviation of error of 5% for the numerical computation of the average Nusselt number. Besides, validation between the present numerical results of the average Nusselt number and suggested correlations are presented in Fig. 5. A good agreement between the numerical results and the proposed correlations is observed.

Single Phase Model (SPM):

$$\overline{Nu} = 0.03930\, Re^{0.76745} Pr^{0.24165} \left(\frac{d_f}{d_p}\right)^{-0.0007074}$$

Multi-phase Model (MPM):

$$\overline{Nu} = 0.037768\, Re^{0.76536} Pr^{0.26123} \left(\frac{d_f}{d_p}\right)^{-0.0062903}$$

where

$2300 \le Re \le 10 \times 10^3,\ 8.45 \le Pr \le 20.29,\ 10 \le d_p(nm) \le 40,\ 0 < \chi(\%) \le 6.$

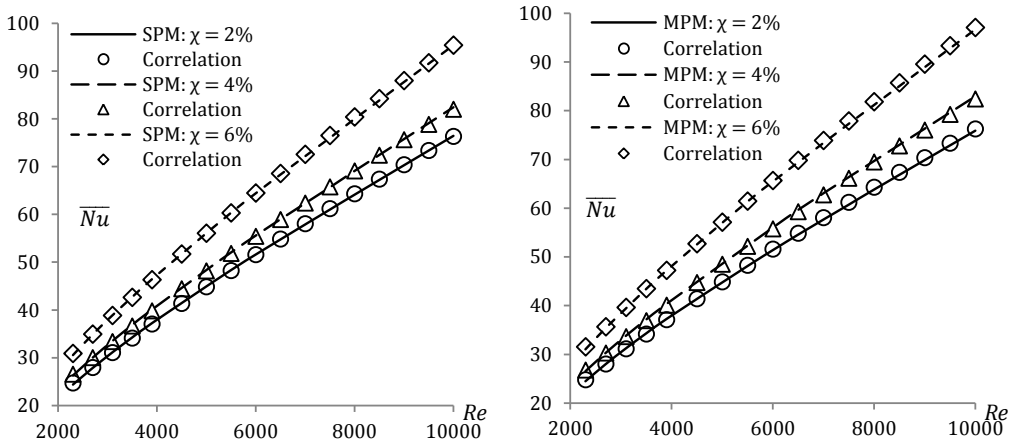

Figure 5: Validation of the proposed correlations with the numerical results for TiO_2-water nanofluid and d_p = 10 *nm* using single phase and multi-phase model

4. Conclusion

In the present analysis, heat transfer and entropy generation behaviour of transition nanofluid flow inside a circular pipe is investigated using both single and multi-phase models. It is observed that addition of smaller nanoparticles in the base fluid (water) helps to enhanced heat transfer rate. Such enhancement is always found higher for multi-phase model than the single phase model. It is also found that there exists no Re such that total entropy generation can be optimized. At the end, two new correlations are proposed for the calculation of average heat transfer rate.

Nomenclature

β_1, β_2	Model constants
C_p	Specific heat capacity (J/kg K)
D_h	Diameter of a pipe (m)
d_f	Fluid molecular diameter (m)
d_p	Diameter of nanoparticle (nm)
E_{gen}	Entropy generation (W/K)
F_1, F_2	Blending functions
f	Darcy friction factor
G_κ	Generation of turbulent kinetic energy
G_ω	Production of ω
H	Enthalpy (J/kg)
I	Turbulent intensity
L	Length (m)
$\dot{m}$	Mass flow rate (kg/s)
N_x, N_r	Number of grid distribution in axial and radial directions
Nu	Nusselt number
P	Pressure (N/m^2)
Pr	Prandtl number
$\dot{q}_s$	Heat flux of the pipe (W/m^2)
Re	Reynolds number
T, t	Time average and fluctuating temperature (K)
V, v	Time average and fluctuating velocity components (m/s)
Greek symbols	
ρ	Density (kg/m^3)
μ	Dynamic viscosity (kg/ ms)
λ	Thermal conductivity (W/m K)
κ	Turbulent kinetic energy (m^2/s^2)
ω	Specific rate of turbulent dissipation (m^2/s^3)
μ_t	Turbulent molecular viscosity
σ_κ	Effective Prandtl number for turbulent kinetic energy
σ_ω	Effective Prandtl number for specific rate of dissipation
χ	Nanoparticle volume concentration
Subscripts	
avg	Average
m	Mixture
s	Secondary phase

References

[1] S. Choi, Enhancing thermal conductivity of fluids with nanoparticles, In Developments and Applications of Non-Newtonian Flows, ASME, FED. 231/MD 66 (1995) 99–105.

[2] S.Z. Heris, M.N. Esfahany, S.G. Etemad, Experimental investigation of convective heat transfer of Al_2O_3/water nanofluid in circular tube, Int. J. Heat Fluid Flow. 28 (2007) 203–210.

[3] K.S. Hwang, S.P. Jang, S.U.S. Choi, Flow and convective heat transfer characteristics of water-based Al_2O_3 nanofluids in fully developed laminar flow regime, Int. J. Heat Mass Transf. 52 (2009) 193–199.

[4] K.B. Anoop, T. Sundararajan, S.K. Das, Effect of particle size on the convective heat transfer in nanofluid in the developing region, Int. J. Heat Mass Transf. 52 (2009) 2189–2195.

[5] E. Esmaeilzadeh, H. Almohammadi, S.N. Vatan, A.N. Omrani, Experimental investigation of hydrodynamics and heat transfer characteristics of Al_2O_3/water under laminar flow inside a horizontal tube, Int. J. Therm. Sci. 63 (2013) 31-37.

[6] S.E.B. Maıga, S.J. Palm, C.T. Nguyen, G. Roy, N. Galanis, Heat transfer enhancement by using nanofluids in forced convection flows, Int. J. Heat Fluid Flow. 26 (2005) 530–546.

[7] E.E. Bajestan, H. Niazmand, W. Duangthongsuk, S. Wongwises, Numerical investigation of effective parameters in convective heat transfer of nanofluids flowing under a laminar flow regime, Int. J. Heat Mass Transf. 54 (2011) 4376–4388.

[8] J. Bayat and A.H. Nikseresht, Investigation of the different base fluid effects on the nanofluids heat transfer and pressure drop, Heat Mass Transf. 47 (2011) 1089–1099.

[9] M.K. Moraveji, M.Darabi, S.M.H. Haddad, R. Davarnejad, Modeling of convective heat transfer of a nanofluid in the developing region of tube flow with computational fluid dynamics, Int. Commun. Heat Mass Transf. 38 (2011) 1291–1295.

[10] S. Mirmasoumi and A. Behzadmehr, Effect of nanoparticles mean diameter on mixed convection heat transfer of a nanofluid in a horizontal tube, Int. J. Heat Fluid Flow. 29 (2008) 557–566.

[11] Y. He, Y. Mena, Y. Zhao, H. Lu, Y. Ding, Numerical investigation into the convective heat transfer of TiO_2 nanofluids flowing through a straight tube under the laminar flow conditions, Appl. Therm. Eng. 29 (2009) 1965–1972.

[12] M.H. Fard, M.N. Esfahany, M.R. Talaie, Numerical study of convective heat transfer of nanofluids in a circular tube two-phase model versus single-phase model, Int. Commun. Heat Mass Transf., 37 (2010) 91–97.

[13] K.V. Sharma, L.S. Sundar, P.K. Sarma, Estimation of heat transfer coefficient and friction factor in the transition flow with low volume concentration of Al_2O_3 nanofluid flowing in a circular tube and with twisted tape insert, Int. Commun. Heat Mass Transf. 36 (2009) 503-507.

[14] M. Chandrasekar, S. Suresh, A.C. Bose, Experimental studies on heat transfer and friction factor characteristics of Al_2O_3/water nanofluid in a circular pipe under transition flow with wire coil inserts, Heat Transf. Eng. 32 (2011) 485-496.

[15] M.T. Naik, G.R. Janardana, L.S. Sundar, Experimental investigation of heat transfer and friction factor with water–propylene glycol based CuO nanofluid in a tube with twisted tape inserts, Int. Commun. Heat Mass Transf. 46 (2013) 13-21.

[16] J.P. Meyer, T.J. McKrell, K. Grote, The influence of multi-walled carbon nanotubes on single-phase heat transfer and pressure drop characteristics in the transitional flow regime of smooth tubes, Int. J. Heat Mass Transf. 58 (2013) 597–609.

[17] C.C. Tang, S. Tiwari, M.W. Cox, Viscosity and Friction Factor of Aluminum Oxide–Water Nanofluid Flow in Circular Tubes, J. Nanotechnol. Eng. Med. 4 (2013) 1-6.

[18] Fluent 6.3 user guide, Fluent Inc., Lebanon, 2006.

[19] F.R. Menter, Two-equation eddy-viscosity turbulence models for engineering applications, J. AIAA 32 (1994) 1598-1605.

[20] E.B. Ratts and A.G. Raut, Entropy generation minimization of fully developed internal flow with constant heat flux, J. Heat Transf. 126 (2004) 656-659.

[21] G. Saha and M.C. Paul, Numerical analysis of heat transfer behaviour of water based Al_2O_3 and TiO_2 nanofluids in a circular pipe under the turbulent flow condition, Int. Commun. Heat Mass Transf., 56 (2014) 96-108.

[22] H. Blasius, Grenzschichten in Flussigkeiten mit kleiner reibung (German), Z. Math. Physics. 56 (1908) 1-37.

[23] V. Gnielinski, New equations for heat and mass transfer in turbulent pipe and channel flow, Int. Chem. Eng. 16 (1976) 359-368.

[24] J.P. Abraham, E.M. Sparrow, J.C.K. Tong, Heat transfer in all pipe flow regimes: laminar, transitional/intermittent, and turbulent, Int. J. Heat Mass Transf. 52 (2009) 557-563.